

Cherenkov τ Shower Earth-Skimming Method for PeV-EeV ν_τ Observation

Y. Asaoka^a, M. Sasaki^a

^a*Institute for Cosmic Ray Research, University of Tokyo,
Kashiwa, Chiba 277-8582, Japan*

Abstract

We describe a method of observation for PeV–EeV tau neutrinos using Cherenkov light from decayed tau air shower produced by tau neutrino interactions in the earth. For observational methods utilizing earth-skimming tau neutrino events, highly precise arrival direction determination is key due to the following issues: (1) Clear identification of neutrinos by identifying those vertices originating within the Earth’s surface; (2) Identification of very high energy neutrino sources. The Ashra detector uses uniquely developed light collectors (LCs) which realize both a 42 degree-diameter field-of-view and arcminute resolution. Therefore, it has superior angular resolution in imaging Cherenkov air showers. In this paper, we estimate the sensitivity of and cosmic-ray background resulting from application of the Ashra-1 Cherenkov tau shower observation method. Both data from a commissioning run and a long-term observation (with fully equipped trigger system and one light collector) are presented. Our estimates are based on a detailed Monte Carlo simulation which describes all relevant shower processes from neutrino interaction to Cherenkov signal detection produced by tau air shower. In addition, the potential to determine the arrival direction of Cherenkov showers is evaluated by using the maximum likelihood method. We conclude that the Ashra-1 detector is a unique probe into detection of very high energy neutrinos and its accelerators.

Keywords: high-energy neutrinos, earth-skimming tau neutrino, Cherenkov images, Ashra, CORSIKA, GEANT4, Monte Carlo simulation

1. Introduction

Gamma ray bursts (GRBs), important high energy transient phenomena, are plausible candidate cosmic ray sources up to and including the highest energy regions. Following the identification of GRB970228 with arcminute resolution made by Beppo-Sax satellite [1], understanding of GRBs progressed dramatically owing to the collaboration of satellite-supplied GRB triggers and follow up multi-wavelength observations. As a result, the GRB standard model based on the acceleration in the internal/external shocks was established [2, 3, 4, 5]. On the other hand, observations of GRB and its afterglow made by Swift [6] and Fermi [7] satellites revealed various phenomena which is difficult to explain in the framework of the standard model. To resolve the various complicated aspects of the GRB physics mechanism, we would need “multi-particle astronomy” [8] which uses other particles in addition to photons. In particular, neutrinos are the most important because they probe the optically thick region for electromagnetic components. As we can learn from Beppo-Sax’s success, identifying the source with superior angular resolution enables us to approach the physics mechanism by combining a number of observational results. To realize “multi-particle astronomy”, arcminute resolution would be mandatory requirement in the field of very high energy (VHE) neutrino observation.

The All-sky Survey High Resolution Air-shower detector (Ashra) is a project which primarily aims to observe Cherenkov and fluorescence lights from the lateral and longitudinal developments of very-high-energy (VHE) cosmic-ray air showers in the atmosphere. It uses uniquely developed light collectors (LCs) which realize both a 42 degree-diameter field-of-view (FOV) and arcminute resolution. In particular, it can capture air-shower images with higher precision than ever. It is expected to determine the arrival direction of parent particle with high accuracy.

As to detection methods for VHE neutrinos, there are methods which use water and/or ice as the neutrino target [9, 10], and those which utilize air showers, i.e., the deeply penetrating neutrino air-shower detection technique and recently proposed “Earth skimming tau-neutrino (ν_τ) technique” [11, 12, 13, 14, 15]. Some results have already been

published with the earth-skimming method (for example, see [16]). On the other hand, by combining Cherenkov emission in the optical band and “Earth skimming ν_τ technique” (Cherenkov tau shower earth-skimming method; hereafter referred to as Cherenkov τ shower ES method), we can effectively survey an energy range which is hard to reach in the above mentioned technique. It is possible to archive the maximum sensitivity around 10–100 PeV in which the VHE neutrino signals from GRBs are expected. Figure 1 shows the expected neutrino fluence from nearby GRB. Following Ref. [17], the expected fluence from GRB030329 is scaled to different redshifts(z). The expected sensitivities of Ashra-1 detector by using Cherenkov τ shower ES method are also plotted in the figure. The sensitivity

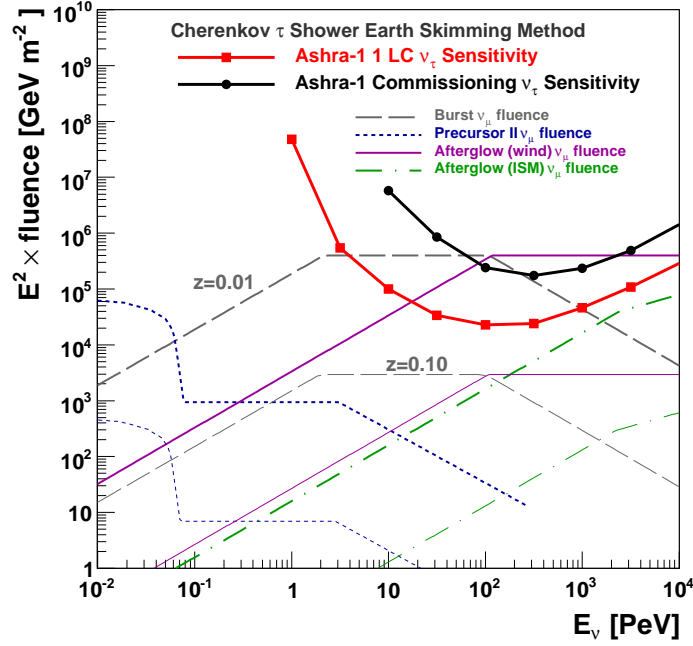


Figure 1: The sensitivity of Cherenkov τ shower ES method with Ashra-1 (see the text). Solid square shows the differential sensitivity of the Ashra-1 observation using one light collector and solid circle shows that of the commissioning observation. Note that differential sensitivity represents the fluence where 2.3 events are expected at the corresponding energy decade. Also shown are the scaled neutrino fluence expected from GRB030329 occurred at $z = 0.01$ and $z = 0.1$ in each phase of GRB [17]. The dashed, dotted, solid and dash-dotted lines show the components of burst, precursor, afterglow in wind environment, and afterglow in ISM environment, respectively.

calculation is performed by using the Monte Carlo simulation described in detail in this paper.

This paper is organized as follows: Section 2 introduces the Ashra-1 detector, Section 3 describes the detailed method to simulate earth-skimming ν_τ events, including the discussion about the deflection during their propagation. Section 4 shows the result of sensitivity estimation. Section 5 discusses the systematic errors due to the incorporated Monte Carlo simulation, background estimation and angular reconstruction accuracy of τ shower events. We conclude in Section 6.

2. Ashra-1 Detector

The All-sky Survey High Resolution Air-shower detector Phase I (Ashra-1) is an optical-telescope based detector system [18] optimized to detect VHE particles. Ashra-1 has two distinguishing features: (1) the ultra wide optical system in which 42-degree FOV is demagnified to 1 inch by using photon and electron optics [19]; (2) the high resolution imaging system with trigger. Ashra-1 combines these unique features, resulting in very cost-effective pixels compared to conventional photomultiplier arrays at the focal surface of an optical telescope. Ashra-1 can observe the

whole sky with arcminute resolution by orienting LCs in twelve directions. Ashra-1 detector system is designed so that the focal image is split into trigger/image capture devices after amplification. This feature enables us to simultaneously obtain 3 kind of phenomena which have different time scales, i.e., Cherenkov emission (ns), fluorescence (μ s), and starlight (s) without sacrificing the signal to noise ratio. By fully utilizing these distinct features, Ashra is aiming to undertake the full-fledged astronomical observation using VHE particles and commencing with the first detection of VHE neutrinos using the earth and the mountain as the target [20]. It can also be used to optically observe transient objects like GRBs as it monitors the whole sky simultaneously [21, 22].

3. Earth Skimming Tau Neutrino

3.1. Neutrino detection method

To detect VHE neutrinos, a large target volume is required in order to compensate for the very small neutrino-nucleus cross section. On that basis, the secondary particles produced by the first neutrino interaction are required to be detected in one way or another. The detection method using water and ice as a target detects Cherenkov light from secondary muons taking advantage of the fact that ice and water are to some extent optically transmissive. This method can be categorized as the method in which target and detection volume are identical. On the other hand, the detection method using air showers aims at the detection of higher-energy neutrinos. This method enables us to achieve a huge detection volume as the atmosphere has very high transmittance. However, it is difficult to obtain a larger target mass due to low atmospheric density. The detection method called earth-skimming ν_τ technique [11, 12, 13, 14, 15] can realize a huge target mass and detection volume at the same time by dividing the target and detection volume utilizing the interaction process of ν_τ . The detection method is described as follows (See Fig. 2). VHE ν_τ interacts in the earth or mountain and produces tau lepton (τ). τ penetrates the earth and/or mountain and appears in the atmosphere. Subsequently, it decays and produces an air shower. Cherenkov photons from the air shower are detected. Owing to the separation of the first interaction where ν_τ produces τ and τ decay generating air shower, air shower observation become possible while preserving the huge target mass required for the first interaction. “Cherenkov τ shower ES method” is defined as the detection method which detects Cherenkov photons from tau shower appeared from the earth or the mountain fully utilizing this feature. Mauna Kea is over 3,200 km³ in volume and 9.3 tera tons in mass [23].

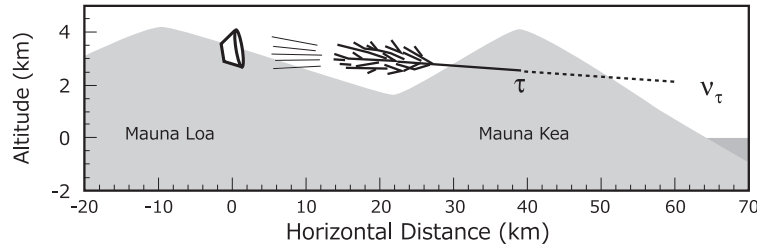


Figure 2: Schematic view of Cherenkov τ shower ES method. Mauna Kea is used as the target mass for neutrino charged current interaction. The produced air shower is observed from Mauna Loa. In addition to the fact that the mountain can be viewed with large solid angle from the observatory, the distance of about 30km from the observatory to the Mauna Kea surface is appropriate for the air shower development, resulting in the huge advantage of the Ashra-1 observatory.

3.2. Deflection from parent tau neutrinos

This section describes deflection of Cherenkov τ shower compared to the arrival direction of parent ν_τ in order to estimate the ability to trace back to the accelerator based on the direction of the detected air shower. We evaluated the deflection of the propagating particle in each step of neutrino charged current interaction, τ propagation in the earth, tau decay, and production of extensive air shower. We used PYTHIA [24] to evaluate neutrino charged current interaction. Since $P_t < M_W$ (where M_W denotes the mass of the W boson which mediates the charged current interaction) and P_t denotes the transverse momentum of a produced τ , the deflection angle of τ ($\Delta\theta_\tau$) with respect to

the parent ν_τ should be less than 0.3 arcmin for $E_\tau > 1$ PeV. The simulation results with PYTHIA were consistent to this.

Second, we used GEANT4[25] to evaluate the τ 's deflection due to propagation in the earth. To estimate the energy loss of high energy leptons, the following parametrization is generally adopted [26]:

$$-\left\langle \frac{dE}{dX} \right\rangle = \alpha + \beta E,$$

where α denotes the nearly constant parameter determined by ionization loss, and β denotes the radiative energy loss due to Bremsstrahlung, pair production and photonuclear interaction. Since radiative energy loss is dominant for high energy τ s, these high energy process must be included in the "Physics List" of GEANT4. Thus, we applied the following processes originally defined for muons to τ s, and estimated the deflection after propagating through 10km rocks.

- G4MuBremsstrahlung: Bremsstrahlung
- G4MuPairProduction: e^+e^- pair production¹
- G4MuNuclearInteraction: Photonuclear Interaction

To validate our GEANT4 simulation, we compared the energy dependence of β for Bremsstrahlung, pair production, and photonuclear interaction to Ref. [26]. The β energy dependence agreed well for the former two processes, but we found that GEANT4 produced smaller values for photonuclear interaction at higher energy and that the difference was 3 times at 10^8 GeV. Accordingly we wrote a toy Monte Carlo simulation for photonuclear interaction using the formalism of Refs. [27, 28]. In this simulation, the energy dependence of β was reproduced within $\pm 30\%$ accuracy. Figure 3 shows the simulation results of deflection angle of τ s after propagating 10km of rocks. Left panel shows the GEANT4 results including all the high energy processes except for photonuclear interaction, and the right panel shows the results of photonuclear interaction simulated by our "handmade" simulation. These results indicate that photonuclear interaction becomes dominant for deflection at 1 PeV and higher. Note that the decay of τ s was switched off for the above simulations and the hatched histograms indicate that the τ range is less than 10km. For example, the τ range is 4.9 km at 100 PeV. We concluded that the deflection angle of τ s with energy greater than 1 PeV is much less than 1 arcmin.

Next, the deflection due to τ decay is estimated by using the output of TAUOLA[29] taken into account of the τ polarization. From the mass of the τ s, the deflection angle must be less than 1 arcmin if the energy of the secondary particle is higher than 13 TeV. Using the TAUOLA outputs, it was shown that the probability to have the deflection greater than 1 arcmin is quite small from the decay of PeV-energy τ s. We concluded that the deflection angle between decay particles which produce the air shower and parent ν_τ was less than 1 arcmin.

Finally, the direction of the hadron air shower was evaluated using CORSIKA. At the shower maximum, we compared the direction of the parent particle (charged pion) to that of electrons and positrons which are dominant producers of Cherenkov photons. We found that the angle between the average direction of electrons and positrons and parent particle of the air shower was coincident within 0.1° at 1 PeV. In conclusion, we found that the arrival direction of PeV ν_τ s was preserved within 0.1° including the hadron air-shower generation. The accurate reconstruction of arrival direction by means of fine imaging will be a very powerful technique in the determination of the point sources of PeV ν_τ s.

3.3. Monte Carlo simulation

To investigate the neutrino identification capability and sensitivity, it is vital to develop a detailed Monte Carlo simulation which simulates from the neutrino interaction to Cherenkov signal detection produced by decayed τ air showers. The first step is to generate the ν_τ s from the certain area and solid angle which is large enough compared with our detector's detection volume. In this step, τ production due to the charged current interaction of ν_τ , τ propagation

¹we modified the original G4MuPairProduction so that the momentum preserves including the produced particles, resulting in the inclusion of deflection.

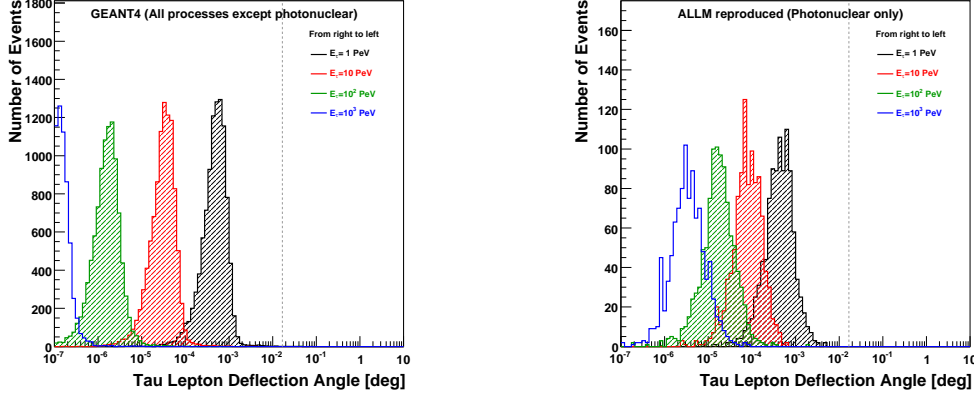


Figure 3: The simulation results of deflection angle of τ s after propagating 10km of rocks. (*Left*) the GEANT4 results including all the high energy processes except for photonuclear interaction. (*Right*) the results of photonuclear interaction simulated by handmade simulation. Note that the decay of τ s was switched off for the above simulations. The hatched histograms indicate that the τ range is less than 10km.

in the earth, and the determination of the decay point of τ s emerging from the earth are simulated. These processes calculates the τ flux emerging from the earth and subsequent decay in the atmosphere. These fluxes are calculated for ν_τ s whose energies range from 10^{15} eV (1 PeV) to 10^{20} eV (100 EeV) in steps of 0.5 decades. The simulation code used in this step is based on the earth skimming ν_τ simulation code described in Ref.[30]. The code is further developed to include mountain effects, and neutrino and τ interactions are updated in part [31]. Considering the direction and energy of τ s emerging from the earth and removing the events with no probability of detection at this step, the efficiency of the simulation was substantially improved.

For the neutrino-nucleus cross section, we used the calculation [32] based on CTEQ4-DIS parton distribution functions (PDFs). Inelasticity is considered by fitting its energy dependence shown in Ref. [33] to a quadratic expression. To estimate the energy losses due to propagation of τ s in the earth, we used the parametrization shown in Ref. [34] based on Ref. [26]. As the density of the earth's crust, we took 2.9 g/cm^3 [35] since the main component of the earth's crust is basalt around Hawaii.

The second step of our simulation consists of τ decay, air-shower generation, and detection in the detector. 4 vectors of secondary particles produced by τ decay were calculated by TAUOLA version 2.4 [29]. The polarity of τ was set to -1 [30]. The decay mode was determined for each τ obtained in the first step, resulting in 1–4 secondary particle(s). Then, an air shower was generated taking into account physical relationship between the air shower and the detector. We used CORSIKA [36] to simulate air showers. Since high energy air-shower generation requires great amount of CPU power, we used a thinning algorithm. To keep the fineness of the shower image taken by the detector as much as possible, we adopted a smaller value of the thinning level $= 10^{-7}$. We used QGSJET [37] as a high-energy hadron interaction model. In CORSIKA, incoming photons to the detector's FOV were recorded by using the IACT package ², and used in the detector simulation. The detector simulation incorporated the light collection area obtained by ray trace of the optical system, measured transmittance, and quantum efficiency of photoelectric lens image intensifier tube. Trigger decision and acquisition of fine images were carried out in this step. Since CORSIKA output includes the generation height and wavelength of detected Cherenkov photons, attenuation in the atmosphere was considered here.

Figure 4 shows the examples of neutrino shower events in the commissioning observation obtained by the Monte Carlo simulation described above. The unique capabilities of the Ashra detector enabled us to obtain unmatched detailed images of Cherenkov showers. In the commissioning observation, we used a limited 62 channels of photo multipliers as trigger sensors to cover the view of the surface area of Mauna Kea as much as possible to maximize the sensitivity [20]. Adjacent-two logic was adopted to trigger the fine imaging to reduce the background events due

²Since the IACT package in CORSIKA ver. 6.900 cannot receive the thinning information correctly, we fixed it to use in our simulation.

to the fluctuation of night sky background and etc. In the Ashra-1 observation with final configuration, the trigger pixel size will be halved (to one quarter of the current pixel area) and the entire FOV of the LC will be covered by the trigger sensor.

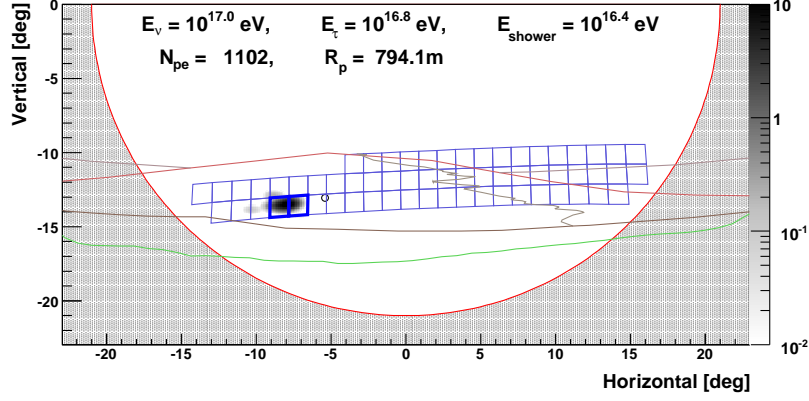


Figure 4: An example of the neutrino shower image obtained by the detailed Monte Carlo simulation with the configuration of commissioning observation.

4. Sensitivity

The effective area (A_{eff}) is calculated for each ν_τ energy (E_{ν_τ}) ranging from 1 PeV to 100 EeV in steps of 0.5 decades. At first, from the direction of the point source, N_{total} ν_τ events are uniformly generated in the large area (A_{eff}^0) containing Mauna Kea. Assuming that N_{det} are finally triggered and detected from N_{total} events, the following equation gives $A_{\text{eff}}(E_{\nu_\tau})$ as a function of neutrino energy.

$$A_{\text{eff}}(E_{\nu_\tau}) = A_{\text{eff}}^0 \frac{N_{\text{det}}(E_{\nu_\tau})}{N_{\text{total}}(E_{\nu_\tau})}.$$

The left panel of Figure 5 shows an overlay of the effective area of 1-LC and the commissioning observations assuming typical point source coordinates with altitude -1.0° and azimuthal angle 17.1° . The commissioning observation used the measured trigger threshold described in Ref.[20], and 1-LC observation used the trigger threshold of 20 photoelectrons. Both cases adopted adjacent-2 trigger logic. On the other hand, right panel of Figure 5 shows the effective aperture for a diffuse neutrino source where the neutrino direction and incident position are uniformly scanned. In both cases of point and diffuse sources, improved sensitivity of 1-LC observation was achieved due to halved trigger pixel size, dense alignment of trigger pixels and lower trigger threshold.

5. Discussion

5.1. Systematic errors

The dominant systematic errors associated with the sensitivity of Cherenkov τ shower ES method can be summarized as follows:

- neutrino-nucleus interaction cross section;
- τ propagation in the earth;
- density of the earth's crust.

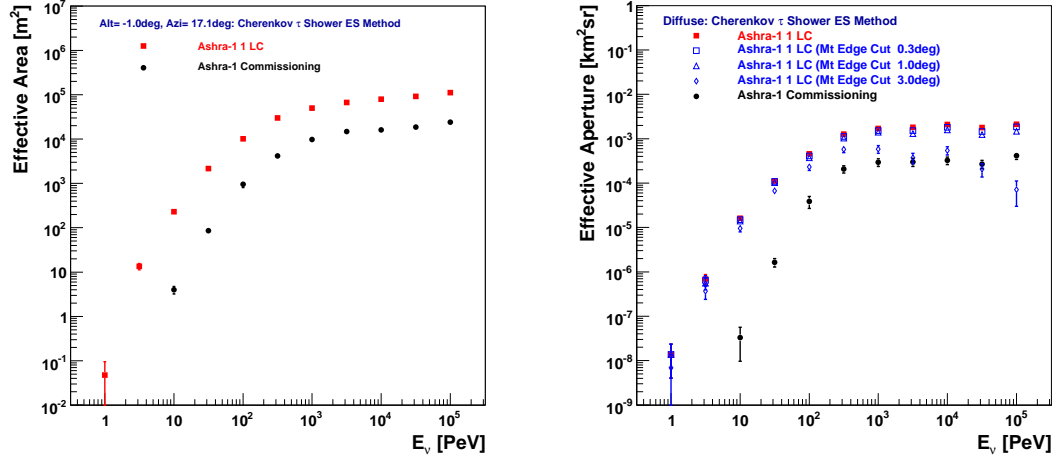


Figure 5: Typical effective area (*Left*) and effective aperture (*Right*) of Cherenkov τ shower ES method with Ashra-1. Effective area was estimated in the case of altitude -1.0° and azimuthal angle 17.1° as an arrival direction of ν_τ s. Red solid squares and black solid circles represent the sensitivity of 1 light-collector observation and the commissioning observation, respectively. Blue open squares, blue open triangles, and blue open diamonds represent the effects of mountain-edge cut of 0.3° , 1.0° , and 3.0° , respectively. For explanation of mountain-edge cut, see the text.

First, the systematic uncertainty of the neutrino-nucleus interaction cross section was addressed. As explained, we used the calculation based on CTEQ4 [32] for the total cross section of neutrino-nucleus interaction. However, it has been pointed out [38, 39] that there is an approximately 50% model uncertainty at 1 EeV due to inconsistency between PDF sets. We took this value as the systematic error of the neutrino-nucleus interaction cross section.

Next, we evaluated the systematic errors of τ propagation in the earth. We used the approach from Refs.[26, 40] to calculate the energy loss by the τ during propagation through the earth and the mountain at PeV energies. The uncertainty in the structure function used in the energy loss calculation defined as the discrepancy between theoretical model predictions of τ 's energy losses at 100 PeV was found to be 50% [40].

Finally, as we did not use typical values for the earth's crust, we considered the uncertainty in crust density itself. Because the incident direction of ν_τ events in the effective FOV was almost horizontal, we adopted the constant value of 2.9 g/cm^3 [41] which is the density of basalt, the dominant component in the surface layer of the earth's crust in the vicinity of Big Island of Hawaii. We took 10% as a conservative systematic uncertainty of the density, which is the difference between the average density of earth's crust (2.6 g/cm^3)[35] and the density of basalt. The conservatively combined systematic sensitivity error was found to be 71% by summing the individual systematic errors in quadrature.

5.2. Angular resolution

From the discussion in Section 3.2, we found that the Cherenkov τ shower of $E > 1 \text{ PeV}$ preserves the arrival direction of the parent ν_τ to within 0.1° accuracy. This means that the detector's ability to reconstruct the arrival direction precisely results in the identification of VHE neutrino source and leads to the realization of "multi particle astronomy". Owing to its high-resolution imaging capability, the Ashra-1 detector has huge potential to improve the reconstruction of tau neutrino Cherenkov shower arrival directions. In this section, shower reconstruction with likelihood analysis will be discussed, where simulated air-shower images are generated with faster Gaisser-Hillas and NKG parametrization [30]. Note that these parametrizations are well established [42, 43].

In this analysis, we adopted the following geometrical reconstruction parameters:

(n_x, n_y) : Shower axis direction in the obtained fine image;

(X', Y') : Intersection of mountain surface with the shower axis (tau emerging point)

E : Shower energy.

(n_x, n_y) and (X', Y') determines the impact point (R_P), and therefore the physical relationship between the detector and the shower axis. Easy and direct comparison between real and simulated data was attained by adopting the positions in the obtained image as the parameters. Here, we used the 100 PeV proton shower to investigate the reconstruction capability and therefore the definition of (X', Y') must be changed. We took the direction of intersection of 25 km height with the shower axis in the image as (X', Y') .

The following geometrical reconstruction parameters were taken as a typical shower example to study the reconstruction accuracy:

$$(n_x, n_y) = (0.0, 0.0) \text{ [deg];}$$

$$(X', Y') = (0.6, 0.0) \text{ [deg];}$$

$$E = 100 \text{ [PeV]}.$$

This parameter set corresponded to $R_P = 540$ m. The left panel of Figure 6 contains an example of the shower image generated with this parameter set. The right panel of Figure 6 shows the probability density distribution obtained by averaging 10^6 events generated with the same parameter set. In this probability density distribution, the longitudinal and lateral development of air shower was calculated using Gaisser-Hillas and NKG, respectively. The direction of Cherenkov photon was calculated by using the parametrization described in Ref. [44]. In this simulation, fluctuation due to first interaction point was taken into account, but air-shower fluctuation due to hadron interaction was not. This effect was accounted for in Section 3.2 (0.1° at 1 PeV). Although it is preferable to include hadron air-shower fluctuation using CORSIKA, generating a sufficient number of events requires an amount of CPU power unavailable during the writing of this paper.

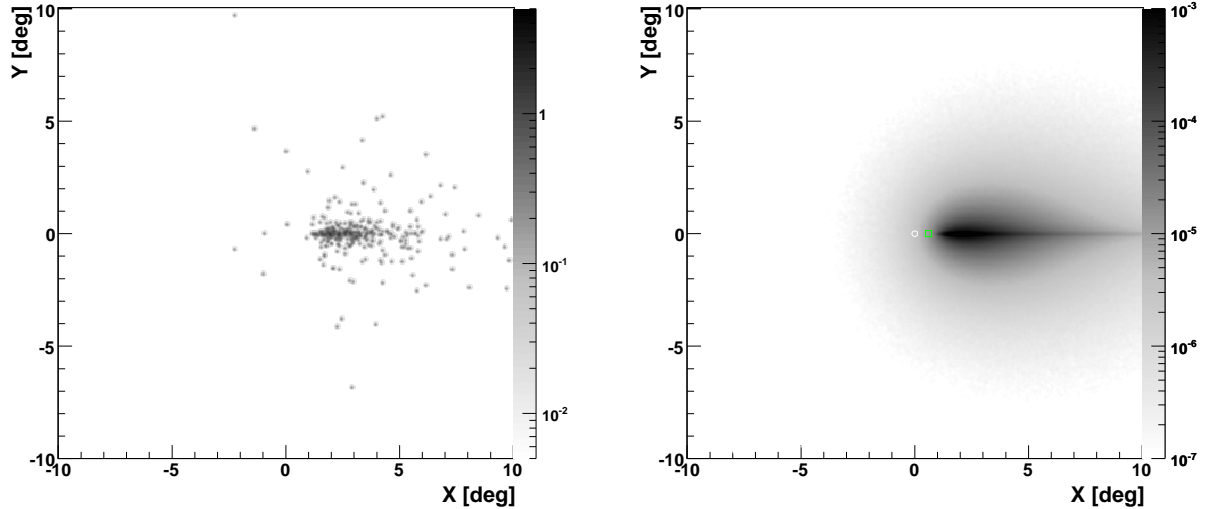


Figure 6: (Left) An example of Cherenkov shower image for event reconstruction, (Right) Probability density distribution. White point represents (n_x, n_y) and green point represents (X', Y') .

Using the number of photoelectrons in pixel i (N_{pe}^i) and the photon detection probability at the pixel (p_i), the likelihood can be written as follows:

$$L = -\frac{1}{2} \sum_i N_{pe}^i \log(p_i). \quad (1)$$

The photoelectron distribution was obtained in the real image and the MC simulation gave the probability density distribution where the geometrical reconstruction parameters were known. Note that the N_{pe}^i in each pixel was not discretized due to the finite resolution of the photoelectric image pipeline.

To estimate errors on the reconstruction parameters, it is necessary to calculate the error matrix for the likelihood defined above. The error matrix is given as the inverse of the second order partial differential matrix of the likelihood as follows:

$$L = L(a_i^*, a_j^*) + \frac{1}{2}(a_i - a_i^*)^2 \frac{\partial^2 L}{\partial a_i^2} + \frac{1}{2}(a_j - a_j^*)^2 \frac{\partial^2 L}{\partial a_j^2} + (a_i - a_i^*)(a_j - a_j^*) \frac{\partial^2 L}{\partial a_i \partial a_j} \quad (2)$$

$$H_{ij} = 2M_{ij} = \frac{\partial^2 L}{\partial a_i \partial a_j} \quad (3)$$

$$R = M^{-1}, \quad (4)$$

where a_i represents the parameter and a_i^* represents the parameter value corresponding to the local minimum. R represents the error matrix, and M represents the second order partial differential matrix. M can be calculated by using the neighborhood values of L around local minimum.

$$\frac{\partial^2 L}{\partial a_i \partial a_j} = \left(L - L(a_i^*, a_j^*) - \frac{1}{2}(a_i - a_i^*)^2 \frac{\partial^2 L}{\partial a_i^2} - \frac{1}{2}(a_j - a_j^*)^2 \frac{\partial^2 L}{\partial a_j^2} \right) \times \frac{1}{(a_i - a_i^*)(a_j - a_j^*)} \quad (5)$$

The inverse of M gives R and, once the error matrix is obtained, the diagonal elements correspond to the parameter errors including correlation between parameters. The errors of shower axis direction (n_x, n_y) are obtained. Using the events generated by the MC simulation as the dummy real data, the reconstruction accuracy of shower axis was evaluated by the inverse matrix calculations described above. The result was 3–5 arcmin, where the error along the shower axis (n_x in this example) dominated. For simplicity, the energy of the shower was fixed during minimization. An example of correlation matrix is shown below.

	n_x	n_y	X'	Y'
n_x	1.00	0.30	0.97	0.21
n_y	0.30	1.00	0.31	0.70
X'	0.97	0.31	1.00	0.21
Y'	0.21	0.70	0.21	1.00

There were strong correlations between n_x and X' . Considering the fact that X' determines R_p , strong correlation between n_x and R_p resulted in a worse joint resolution. This is a well-known problem connected with the mono detection of Cherenkov shower and will be greatly improved in the case of stereo detection. Combining the fine imaging and high statistics, however, it was shown that the reconstruction of shower direction with the accuracy of several arcmin was possible. This analysis outlined the fact that the high-resolution Cherenkov imaging would lead to the high accuracy reconstruction of the arrival direction. The potential of Ashra-1 detector was demonstrated and systematic study will follow.

5.3. Background

In this section, we evaluate the background events due to air showers. Background events due to the detector itself were discussed in Ref. [20]. Air-shower background candidates are normal cosmic rays, muons, muon neutrinos, τ s, and ν_τ s. The large zenith angle components of these candidates must be considered. From simple flux calculations, it was shown that the neutrino components through mountain, prompt τ components and muons were negligible [31, 45, 46, 47, 48]. Thus, the large zenith angle component of normal cosmic rays was considered as the dominant background component in our analysis here.

In this study, CORSIKA was used in the same way with the ν_τ simulation. To consider the atmospheric depth correctly, "CURVED EARTH" option was applied. The IACT package was used to simulate incoming Cherenkov photons. Protons were selected as the parent particle and a thinning parameter of 10^{-5} was adopted. To investigate the zenith angle and the energy dependence of the background flux, the thinning level difference between this simulation and the ν_τ simulation was unavoidable. At first, to estimate the background rate during the commissioning observation, the trigger rate for trigger-pixel alignment adopted in commissioning observation was calculated. As we could not simulate the largest zenith angle (θ_{zen}) of $\theta_{zen} > 88^\circ$ in the combination of "CURVED EARTH" and IACT options,

trigger pixels were offset by two degrees toward higher elevation to estimate the trigger rate for $88^\circ < \theta_{\text{zen}} < 90^\circ$. To account for the trigger rate decrease due to thicker atmospheric depth, the result was further corrected by the ratio of expected events between $84^\circ < \theta_{\text{zen}} < 86^\circ$ and $86^\circ < \theta_{\text{zen}} < 88^\circ$ in the event that the entire FOV was covered by the trigger pixel. As a result, the number of expected background events (N_{CR}) due to normal cosmic rays during commissioning observation of 197.1 hr was estimated to be:

$$N_{\text{CR}} = 1.3 \times 10^{-4},$$

which was small enough to be neglected. Note that the above discussion did not use the cosmic ray event selection using the reconstructed arrival direction information.

Next, the cosmic-ray background in 1-LC observation with final configuration was evaluated. With the maximum weather efficiency of 100%, 1750 hr of observation time is expected in one year. Assuming the trigger pixel threshold of 20 photoelectrons which is the same as for our sensitivity estimation, the cosmic-ray shower event rate emerging from the mountain edge was found to be 8.2×10^{-2} , 0.55, 4.3, 39 (per year) for 0.1° , 0.3° , 1.0° , 3.0° from the mountain edge, respectively. Assuming perfect event reconstruction of the arrival direction, a background-free result was easily achieved by requiring that the reconstructed shower direction was in the mountain or the earth. In practice, the background-free result was achieved by requiring a mountain-edge cut in which the reconstructed arrival direction was inside the mountain edge by θ_{cut} , where θ_{cut} was an angle dependent on the reconstruction accuracy. It is important to evaluate the effective aperture dependence on the mountain-edge cut. By using the neutrino simulation data set, the effective aperture was estimated to be 90%, 80% and 38% for mountain-edge cuts of 0.3° , 1.0° and 3.0° , respectively. The right panel of Figure 5 shows the energy dependence of effective apertures with the mountain-edge cut. Blue open squares, blue open triangles, and blue open diamonds represent the effects of mountain-edge cut of 0.3° , 1.0° , and 3.0° , respectively. The effective aperture with a 3.0° mountain-edge cut was shown to estimate the θ_{cut} dependence of the effective aperture although 3.0° was too large compared with the Ashra-1 angular resolution. The large decrease in the effective aperture at higher energy in 3.0° mountain-edge cut was due to the fact that higher energy neutrinos could only be emerging from the mountain edge because of thinner mountain material. As shown above, the reconstruction accuracy of the arrival direction directly affects the effective aperture of the detector. In addition, it was very important to positively identify the neutrino shower event. The high-resolution imaging capability would be the key feature in the detection of VHE neutrinos for the first time.

6. Conclusion

In the observation of VHE neutrinos from the high energy transient objects, highly precise arrival direction determination is the key in terms of the following points: (1) Clear identification of neutrinos by distinguishing their appearance from the earth; (2) Identification of VHE neutrino point sources. We studied the physical processes of earth-skimming ν_τ s in detail, and found that Cherenkov τ showers of > 1 PeV preserved the arrival direction of the parent ν_τ to within $< 0.1^\circ$ accuracy. The Ashra detector uses uniquely developed light collectors which realize both a 42 degree-diameter FOV and arcminute resolution. It is capable of capturing the high-resolution Cherenkov image with higher precision than ever. Maximizing the effect of fine imaging, the use of maximum likelihood analysis would lead to several arcmin accuracy in the determination of the arrival direction of Cherenkov showers when sufficient photon statistics are obtained. The ‘‘Cherenkov τ shower ES method’’ which detects the Cherenkov photons from τ air shower has the highest point source sensitivity in the 10–100PeV range. These results indicate that the Ashra-1 detector is a unique probe of VHE neutrinos and their accelerators. The first physics results using this method were published in Ref. [20].

Acknowledgment

We thank S. Ogawa, P. Binder and J. Goldman for useful discussion. The Ashra-1 project is supported by the Coordination Fund for Promoting Science and Technology (157-20004100) and by Grant-in-Aid for Scientific Research (19340055, 19403004, 16403001, 23684013) from the Ministry of Education, Culture, Sports, Science and Technology in Japan.

References

- [1] E. Costa, et al., Nature 387 (6635) (1997) 783–785.
- [2] M. J. Rees, P. Meszaros, MNRAS 258 (1992) 41.
- [3] R. Sari, T. Piran, ApJ Lett. 455 (1995) L143.
- [4] T. Piran, Phys. Rep. 314 (1999) 575.
- [5] P. Mészáros, Rep. Prog. Phys. 69 (2006) 2259, and references therein.
- [6] N. Gehrels, et al., ApJ611 (2004) 1005.
- [7] A. A. Abdo, et al., Science 323 (2009) 1688.
- [8] M. Sasaki, Proc. of ICRR2000 Satellite Symposium: Workshop of Comprehensive Study of the High Energy Universe.
- [9] R. Abbasi, et al., ApJ710 (2010) 346.
- [10] R. Abbasi, et al., ApJ701 (2009) 1721.
- [11] G. Domokos, S. Kovesi-Domokos, AIP Conf. Proc. 433 (1998) 390.
- [12] A. Letessier-Selvon, AIP Conf. Proc. 566 (2000) 157.
- [13] H. Athar, G. Parente, E. Zas, Phys. Rev. D62 (2000) 093010.
- [14] D. Fargion, ApJ570 (2002) 909.
- [15] J. Feng, P. Fisher, F. Wilczek, T. Yu, Phys. Rev. Lett.88 (2002) 161102.
- [16] J. Abraham, et al., Phys. Rev. Lett.100 (2008) 211101.
- [17] S. Razzaque, P. Mészáros, E. Waxman, Phys. Rev. D69 (2004) 023001.
- [18] M. Sasaki, J. Phys. Soc. Jpn. 77SB (Supplement B) (2008) 83.
- [19] Y. Asaoka, M. Sasaki, Nucl. Instrum. Methods Phys. Res. A 647 (2011) 34.
- [20] Y. Aita, et al., ApJ736 (2011) L12.
- [21] Y. Aita, et al., GCN Circular, 8632.
- [22] Y. Asaoka, et al., GCN Circular, 11291.
- [23] E. Wolfe, W. Wise, G. Dalrymple, U.S. Geological Survey Professional Paper 1557 (1997) 129.
- [24] T. Sjöstrand, et al., Comput. Phys. Commun. 135 (2001) 238.
- [25] S. Agostinelli, et al., Nucl. Instrum. Methods A 506 (2003) 250.
- [26] S. Iyer Dutta, et al., Phys. Rev. D63 (2001) 094020.
- [27] H. Abramowicz, A. Levy, arXiv:hep-ph/9712415v2.
- [28] B. Badelek, J. Kwiecinski, Rev. Mod. Phys. 68 (1996) 445.
- [29] S. Jadach, et al., Comput. Phys. Commun. 76 (1993) 361.
- [30] M. Sasaki, Y. Asaoka, M. Jobashi, Astropart. Phys. 19 (2003) 37.
- [31] Y. Aita, et al., in: 31th Intl. Cosmic Ray Conf. (Lodz), ID0313, 2009.
- [32] R. Gandhi, et al., Phys. Rev. D58 (1998) 093009.
- [33] R. Gandhi, et al., Astropart. Phys. 5 (1996) 81.
- [34] J. Tseng, et al., Phys. Rev. D68 (2003) 063003.
- [35] A. M. Dziewonski, D. L. Anderson, Physics of the Earth and Planetary Interiors 25 (1981) 297.
- [36] D. Heck, et al., Report FZKA 6019.
- [37] N. Kalmykov, S. Ostapchenko, A. Pavlov, Nucl. Phys. B (Proc. Suppl.) 52B (1997) 17.
- [38] L. Anchordoqui, A. Cooper-Sarkar, D. Hooper, S. Sarkar, Phys. Rev. D74 (4) (2006) 43008.
- [39] E. Henley, J. Jililian-Marian, Phys. Rev. D73 (9) (2006) 094004. doi:10.1103/PhysRevD.73.094004.
- [40] N. Armesto, C. Merino, G. Parente, E. Zas, Physical Review D 77 (1) (2008) 13001.
- [41] W. Mooney, G. Laske, T. Masters, J. Geophys. Res. 103 (B1) (1998) 727–747.
- [42] C. Song, et al., Astropart. Phys. 14 (2000) 7.
- [43] T. Antoni, et al., Astropart. Phys. 14 (2001) 245.
- [44] R. Baltrusaitis, et al., Nucl. Instrum. Methods A 240 (1985) 410.
- [45] E. Zas, et al., Astropart. Phys. 1 (1993) 297.
- [46] R. Enberg, et al., Phys. Rev. D78 (2008) 043005.
- [47] A. Martin, et al., Acta Physica B 34 (2003) 3273.
- [48] H. Athar, et al., Astropart. Phys. 18 (2003) 581.